Journal of Adhesion Science and Technology, 2015
Vol. 29, No. 2, 133–148, http://dx.doi.org/10.1080/01694243.2014.977698

Temperature dependence of microscale adhesion force between solid surfaces using an AFM

Tianmao Lai*, Rongyu Chen and Ping Huang

School of Mechanical and Automotive Engineering, South China University of Technology, Wushan Road 381, Tianhe District, Guangzhou 510640, China

(*Received 14 September 2014; final version received 11 October 2014; accepted 14 October 2014*)

The adhesion force between two solid surfaces is of great interest with the rapid development of micro–nanodevices and instruments. The effect of temperature on the microscale adhesion force has been studied by recording force–displacement curves with an atomic force microscope. A flat tip with a diameter ~1.73 μm was used to prevent wear. The adhesion force measurements were carried out under ambient conditions and in a nitrogen-filled glove box. The substrate temperature was varied between 30 and 200 °C. The results show that when the temperature is <200 °C, the influence of temperature on the normal spring constant of the cantilever can be ignored. In this temperature range, the adhesion force distribution for each temperature exhibits a Gaussian-like distribution under both situations. Under ambient conditions, the mean adhesion force first increases with the increase in temperature and reaches the maximum at ~100 °C. Then the adhesion force begins to decline slightly. At about 150 °C, the adhesion force decreases dramatically, and remains relatively stable at high temperatures. The increase in adhesion force is associated with the capillary force. The elevated temperature leads to larger and more numerous liquid bridges. The capillary nucleation, the diffusion of water molecules, and the flow of thin water film are all enhanced with the elevated temperature. However, in dry nitrogen, the mean adhesion force decreases with the increase in temperature. This trend is attributed to the broken van der Waals bonds.

Keywords: adhesion force; temperature; atomic force microscope; force–displacement curve; microscale; flat tip

1. Introduction

The adhesion force between two solid surfaces is of great interest in many scientific and industrial fields. With the increasing shrink of miniaturized systems, such as micro–nanoelectromechanical systems and magnetic storage devices, this kind of adhesion force becomes more and more important. For small-scale mechanical systems, surface effect becomes the dominant factor influencing mechanical performance due to a high surface-area-to-volume ratio.[1,2] As a consequence, the influence of the adhesion force on the reliability of these systems becomes significant.

An atomic force microscopy (AFM) is commonly used for the investigation of the adhesion force at the micro/nanoscale. Using an AFM, it is simple and accurate to determine adhesion force with high spatial resolution. Adhesion forces between any types of surfaces can be measured in any environment. And the AFM is less subject to

*Corresponding author. Email: laitianmao@163.com

contamination than other apparatuses measuring adhesion force in microscale. The adhesion force is determined by recording a force–displacement curve. The force–displacement curve is obtained by monitoring the deflection of a cantilever as the tip approaches and retracts from the sample surface.

To measure the adhesion force by an AFM, we should always know the tip shape beforehand. A sharp tip usually has a parabolic shape with an end radius varying from 10 to 100 nm. The wear of sharp tips is a serious disadvantage in measuring the adhesion force.[3] Sharp tips wear easily, resulting in the variation of the contact area between the tip and sample. If the real contact area is not well defined, it will be difficult to quantify the adhesion force. The shortcoming can be overcome by the introduction of a probe tip with a large and flat end. However, this kind of tip has only been used in a few experiments to study the adhesion force.[4–9]

Using a flat tip having a square surface measuring 0.7 μm × 0.7 μm, Ando [4] measured the adhesion force and friction force between the tip and the hemispherical asperity arrays on Si produced by focused ion beam. In a subsequent publication, Ando [5] studied the adhesion forces between a Ni tip with a 0.1 μm^2 flat area and a flat Si substrate. Ferreira et al. [6] used a flat probe tip to measure the adhesion force. The results showed that the adhesion force is greatly influenced by the combination of material characteristics, testing geometry, and experimental protocol (contact time, contact force and contact area). Çolak et al. [7] used a flat tip with a diameter of 2 μm to measure the adhesion forces between the tip and a smooth and chemically etched Si (1 0 0) surface. Recently, Çolak et al. [8] used two flat tips to study the influence of some experimental variables (load, contact time, contact area, relative humidity, and retraction speed) on the adhesion forces between two flat surfaces. In a recent work of Lai and Huang [9], the adhesion force measurements between a flat tip and some samples were carried out under ambient conditions, in dry nitrogen, under distilled water, and under potassium chloride solution. The outcome shows that, under different conditions, various interactions and factors affecting adhesion force are mutually coupled to determine the final adhesion force.

It is well known that many factors, such as surface roughness, hydrophilicity, temperature, and humidity, can influence adhesion force. Some factors are well studied. However, there are only a few studies concerning the influence of temperature on adhesion force.[10–14] Some researchers found that the adhesion force will decrease with increasing temperature. For example, Nelson et al. [10] studied the capillary force between an AFM tip and mica at various temperatures. The results showed that at low humidity, the capillary force decreases with increasing surface temperature, and this is attributed to water evaporation off the heated surface. Tambe and Bhushan [11] studied the adhesion force of four samples in humidity environment and found that the adhesion force decreases as the temperature increases (between 20 and 125 °C). This trend was attributed to the desorption of water molecules and the reduction of water surface tension. Awada et al. [12] reported the adhesion force between an AFM tip and the cross-linked polydimethylsiloxanes. Temperature was varied between 30 and 140 °C. They found out that the adhesion force decreases when the temperature increases, and it was attributed to the decrease in the intermolecular interactions between the tip and the surface. Shavezipur et al. [13] studied the adhesion force between polycrystalline silicon surfaces at elevated temperatures by introducing new microstructures. They found that in the absence of electrostatic and capillary forces, the adhesion force is notably reduced. However, Cappella and Stark [14] observed an increase in the adhesion force with increasing temperature for a contact between the AFM tip and a

polymer film. Their results showed that the temperature dependence of the adhesion force is a consequence of the temperature dependence of the stiffness and of the elastic–plastic properties of the sample. It can be seen that the temperature dependence of the adhesion is still not conclusive.

In this paper, the influence of temperature on the microscale adhesion force will be studied by recording force–displacement curves with an AFM. The varied temperatures are achieved by heating the substrate. The substrate temperature was varied between 30 and 200 °C. A flat tip will be used to measure the adhesion forces of a rough silicon wafer for different temperatures under ambient conditions and in dry nitrogen. The influence of temperature on the normal spring constant of the cantilever will be studied. In order to obtain mean adhesion forces and the distribution, a number of locations will be selected to record adhesion forces in a scanning area. The mean adhesion forces and the distributions will be investigated to analyze how the temperature will influence the adhesion force behaviors. And the reason why we obtain these adhesion force behaviors will be discussed. The results of this paper can provide a reference to the design and manufacture of micro–nanodevices and instruments.

2. Experimental details

2.1. *Sample preparation and characterization*

The sample (grooved Si) is ground from a polished silicon wafer by a grinding wheel with diamond particles.[15] The polished silicon wafer is an N-type wafer of (100) orientation. The thickness is 400 ± 10 μm, and the resistivity is 5–10 Ω cm. An area of 60 × 60 μm^2 was selected as a representative of the sample. The surface topography of the sample has been determined using the contact mode of the AFM, as shown in Figure 1. The surface height distribution of the sample is a Gaussian-like distribution. The average roughness is ~30 nm and root-mean-square roughness is ~37.4 nm. The contact angle with water is 21.9 ± 2.4°, and the surface free energy is ~62.8 mJm^{-2}. Before the experiments, the sample was ultrasonically cleaned in an alcohol solution for 15 min, and then ultrasonically cleaned in distilled water for 15 min.

2.2. *Adhesion force measurement method*

The experiments were performed using an AFM of beam deflection type (AFM, Being Nano-Instruments CSPM-4000, China). The microscope can be operated under ambient

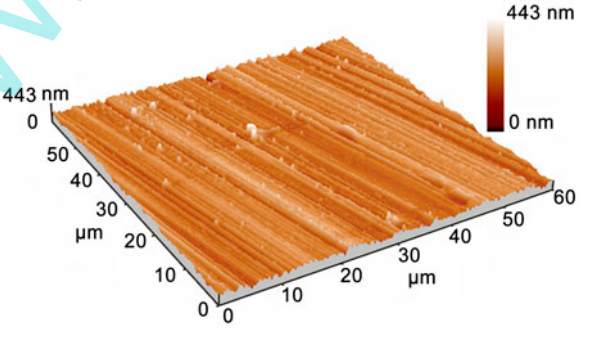

Figure 1. The topography of the sample measured by the AFM.

conditions and in a nitrogen-filled glove box (Etelux Lab2000) where the water content and oxygen content are all less than 0.1 ppm.

A single crystalline silicon probe (PL2-CONTR by Nanosensors, Switzerland) with a flat tip was used in the experiments. The tip shape (as shown in Figure 2) and other geometric values of cantilevers were determined using a scanning electron microscopy (SEM, FEI Nova Nano 430). An intentionally blunt tip with a well-defined circular end-face is located at the free end of a rectangular cantilever. The flat tip is formed by focused ion beam milling and has a ~1.73 μm diameter contact area. The normal spring constant C_N of the cantilever can be calculated as [16]:

$$C_N = \frac{Ewt^3}{4l^3} \tag{1}$$

where E is the elastic modulus, w, t, and l are the width, thickness, and length of the cantilever, respectively. The normal spring constant of the probe used here is ~0.135 Nm^{-1}. It is worthwhile to note that only if the normal spring constant is sufficiently low, the adhesion force measured by the AFM corresponds to the maximum attractive force.[17] That is why we choose a soft cantilever. One shortcoming of the soft cantilever is that the maximum adhesion force detected cannot be very large, since the bending deflection of the cantilever is limited. This is why we use the grooved Si (the adhesion force is decreased due to smaller real contact area) instead of the polished silicon wafer.

In the AFM, adhesion force measurements are performed by recording force–displacement curves. A typical force–displacement curve is shown in Figure 3. The approaching and retracting processes is from point A to point H. (A–B) The sample is initially far away from the probe tip, and no measurable interaction is detected between them. This segment is regarded as the zero line. Upon approaching the surface, the end of the cantilever may bend downward or upward (not shown in the figure) due to the attractive or repulsive forces. (B–C) If the short-range attractive force gradient of the tip–sample interaction exceeds the normal spring constant of the cantilever, the tip will snap into contact with the sample. (C–D) The tip–sample interaction continues to increase as the sample moves upward, until a predetermined maximum normal load is reached. (D–E) The retraction of the sample will lead to the decrease in the interaction.

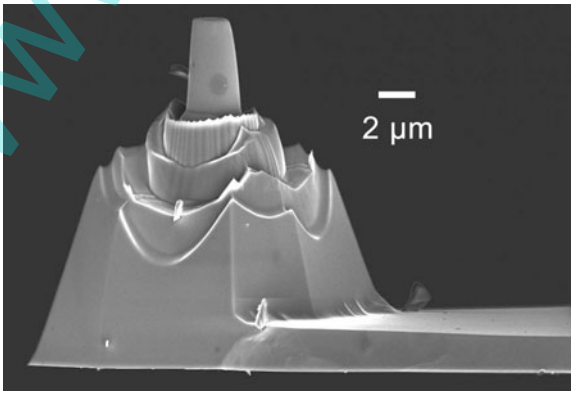

Figure 2. SEM image of the flat tip.

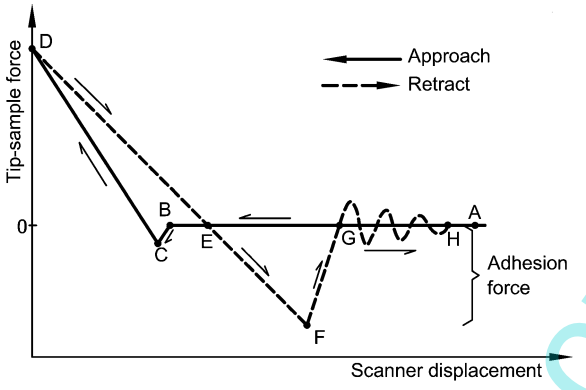

Figure 3. A schematic of a typical force–displacement curve with highlights of the various stages (A–H) of the tip as it is brought into and out of contact with the sample at a fixed point.

(E–F) The tip keeps in contact with the sample because of the adhesion force with the withdrawal of the sample. (F–H) When the normal spring constant overcomes the attractive force gradient, the cantilever snaps back to its original undeflected position with vibration. The vibration reduces gradually and completely disappears after a short span of time.

2.3. *Heating unit*

In the AFM system, a heating unit was installed on the scanner to elevate the temperature of the substrate. As shown in Figure 4, the unit mainly consists of wire terminal, the base, cooling fins, and sample holder. The cooling fins are used to dissipate the heat

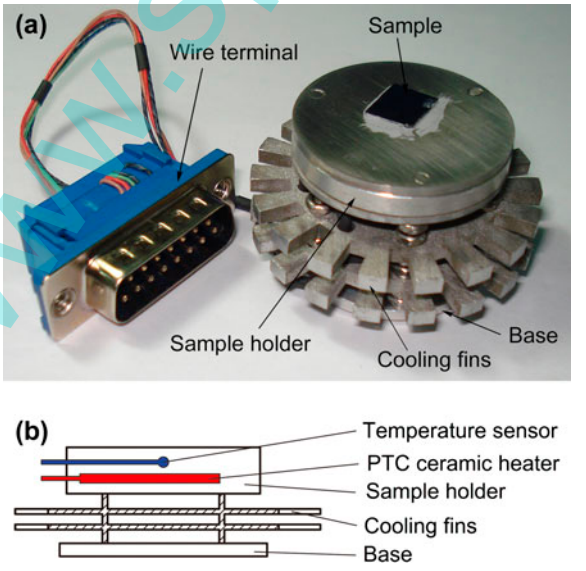

Figure 4. (a) Photograph and (b) schematic diagram of the heating unit of the AFM.

to avoid the damage of the scanner. The sample holder is made of magnetic stainless steel. There is a precision integrated-circuit temperature sensor (LM35, National Semiconductor) just under the upper surface of the holder. And a positive temperature coefficient (PTC) ceramic heater is also inside the holder. A thin layer of thermal conductive silicone grease (ShinEtsu X-23-7783D) was added between the sample and the holder to decrease the thermal contact resistance. The coefficient of thermal conductivity of the grease is larger than 6 $W(mK)^{-1}$. The temperature of the holder can be set on a controller connecting to the AFM. The substrate temperature can be varied from room temperature to 200 °C. The temperature error is less than 3 °C.

Before the measurement, the tip and sample were in contact with a certain loading force. Then the tip was elevated by driving the screws which support the probe base until the distance of the tip and sample is a few micrometers. The controller is turned on to heat the sample. The heat of the sample is transferred to the tip across the tip-substrate air gap. With the increase in the temperature, the end of the cantilever will bend downward due to the deformation of the cantilever and/or the attractive forces. This leads to the movement of the laser spot on the quadrant photodetector. After a few minutes, the laser spot should be adjusted when the temperature of the probe is stable. Then the tip can be approached to contact with the sample. The adhesion force tests can be performed after the temperature of the probe is almost the same as that of the sample. This process will take a few minutes too.

3. Results and discussion

3.1. *Influence of the temperature on normal spring constant*

The determination of the spring constant of the cantilever is of fundamental importance to users of the AFM. In the measurement of adhesion forces at varied temperatures, a question is whether the normal spring constant will be changed by the increased temperature. It can be seen from Equation (1) that the normal spring constant depends on the elastic modulus and geometric values of the cantilever. Since the linear thermal expansion coefficient of silicon below 200 °C is so little, the expansion of the cantilever can be ignored.[18] The elastic modulus of silicon will not be changed largely by increased temperature. For example, the elastic modulus is 169.0 GPa at 25.1 °C, and 166.2 GPa at 151.5 °C for the [1 1 0] direction of silicon.[19] Therefore, the normal spring constant is viewed as a constant in this work. And this assumption is confirmed in our experiments.

The natural frequency of the cantilever can be obtained by recording force–displacement curves at varied temperatures. After the tip snaps out of contact with the sample, the vibration of the tip can be simplified as an underdamped linear vibration of a one-degree-of-freedom system. To make sure that the temperature of the cantilever is almost the same as the sample, the tip was contacted with the sample for about two minutes before the measurement. Five force–displacement curves were collected for each temperature. For each curve, the number of the sampling points was 8000, and the delay time for each point was 1 μs, and the dwell-in time was 0 s. Since the delay time is the same as the sampling period, a force–displacement curve can be changed into a force–time curve. The inset of Figure 5 shows a segment of a typical force–time curve. Then the period of vibration can be obtained from the force–time curve. The cantilever oscillates at the natural damped frequency $f = \left[\left(1-\zeta^2\right)C_N/m_c\right]^{1/2}/(2\pi)$, where ζ is the damping ratio and m_c is the mass of the cantilever.[20] If the damping ratio is assumed as a constant, the normal spring constant is proportional to the f^2.

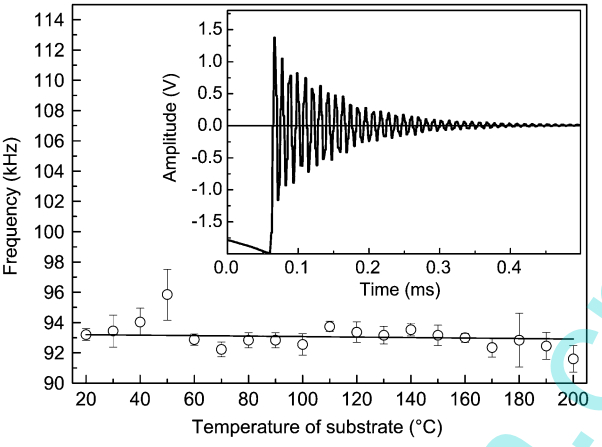

Figure 5. Natural damped frequency of the cantilever vs. temperature of substrate. Each data point represents the average value of five measurements, and vertical error bars represent the standard deviation. The inset shows a segment of a typical force–time curve reflecting the vibration of the cantilever.

Figure 5 shows that the natural damped frequency remains in the vicinity of 93 kHz with the increase in the substrate temperature (the resonance frequency is ~190 kHz from the tuning process of the AFM). Therefore, the normal spring constant will not be changed with the increase in temperature.

3.2. *Influence of temperature on the adhesion*

The experiments were carried out under ambient conditions (ambient temperature 29 ± 1 °C, relative humidity 55 ± 5%) and in the glove box (ambient temperature 31 ± 1 °C, water content <0.1 ppm). To study the influence of temperature on the adhesion, the heating unit was connected to the scanner, and the sample was placed on the sample holder. The sample temperature can be changed between 30 and 200 °C. A group of force–displacement curves were obtained for different temperatures. In a scanning area of 60 μm × 60 μm, 1024 uniformly distributed locations were selected. A force–displacement curve was recorded for every location. The maximum applied load is ~220 nN, the loading rate is ~405 nNs^{-1}, the retraction velocity of the tip is 3 μms^{-1}, and the dwell-in time is 0 s. Due to the fluctuation of the temperature and heat dissipation of the sample and the probe, these parameters will be influenced to some extent. In the experiments, some scanning areas were selected at each temperature. Finally, the adhesion forces were obtained from all the force–displacement curves. The statistics of the adhesion forces were carried out, and the average value and standard deviation were calculated.

When the temperature is relatively high, some force–displacement curves are not correct when collecting curves in a large area. It means that the curves do not have the typical features of a force–displacement curve. The incorrect curves are not obtained when the temperature is relatively low. Therefore, high temperature may be the main reason of the incorrect curves. For one thing, the heat of the holder, the sample and the probe will dissipate into the air or the nitrogen atmosphere. The tip will be separated with the sample once when collecting a force–displacement curve. Therefore, the

temperature of the cantilever will change with time. When the tip is far away from the surface, the position of the tip is variable. That means the position of the laser spot on the quadrant photodetector will change when the tip is far away from the sample. However, the range of the scanner (moving up and down) is settled at the beginning of the experiments. And the voltage of the quadrant photodetector is also limited to ±2 V due to large non-linearity at high voltages. Therefore, with the retraction of the scanner, the tip may not snap out of contact with the sample surface. Or with the extension of the scanner, the tip may not snap into contact with the sample surface. Or the voltage of zero line is so close to −2 V that the photodetector voltage is off the scale when the tip touches the sample. Figure 6 shows three force–displacement curves obtained at different temperatures under ambient conditions. For convenience, the *Z* voltage of the scanner and the voltage of photodetector are used as the variables of the coordinates.

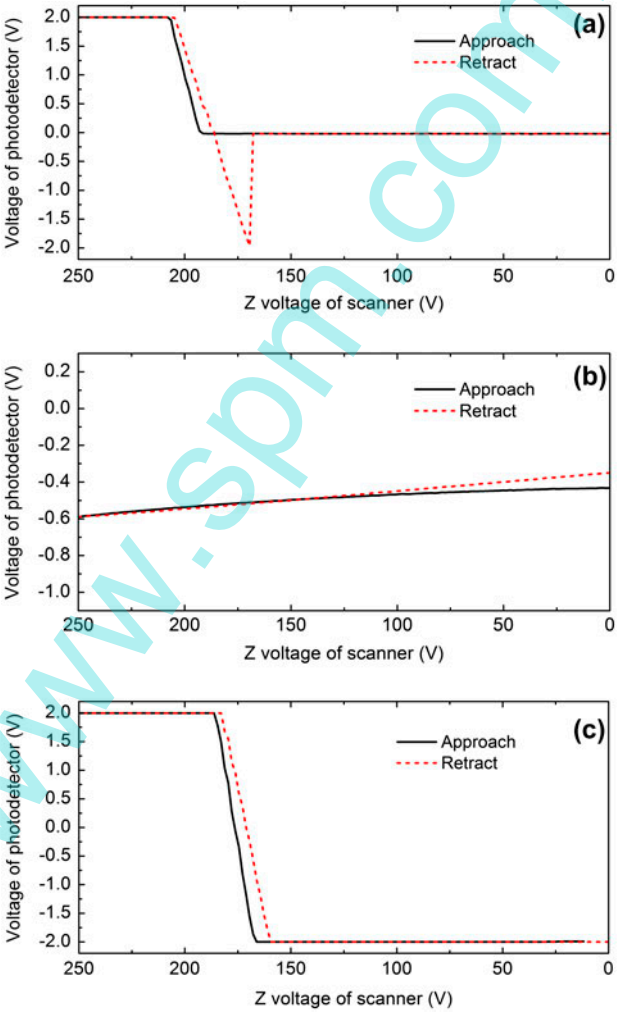

Figure 6. Three force–displacement curves obtained under ambient conditions. (a) Typical curve at 30 °C; (b) incorrect curve at 130 °C; and (c) incorrect curve at 170 °C.

They are in proportion to the scanner displacement and the tip-sample force, respectively. As shown in Figure 6(a), the curve was obtained when the temperature was

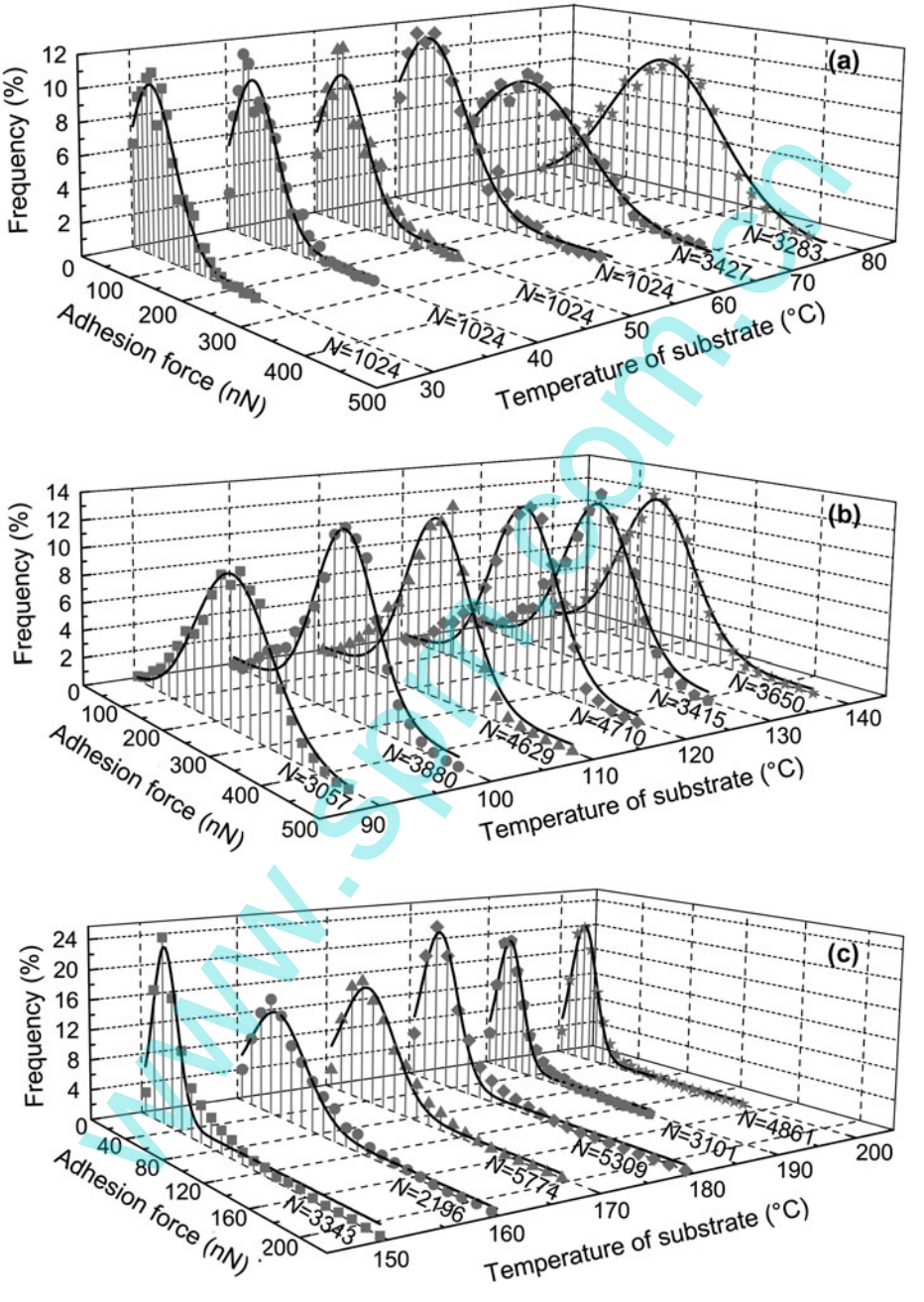

Figure 7. Histograms that show the distribution of adhesion force values quantified for different temperatures under ambient conditions. (a) The temperatures are between 30 and 80 °C; (b) the temperatures are between 90 and 140 °C; and (c) the temperatures are between 150 and 200 °C. The numbers of the curves used are displayed beside the histograms.

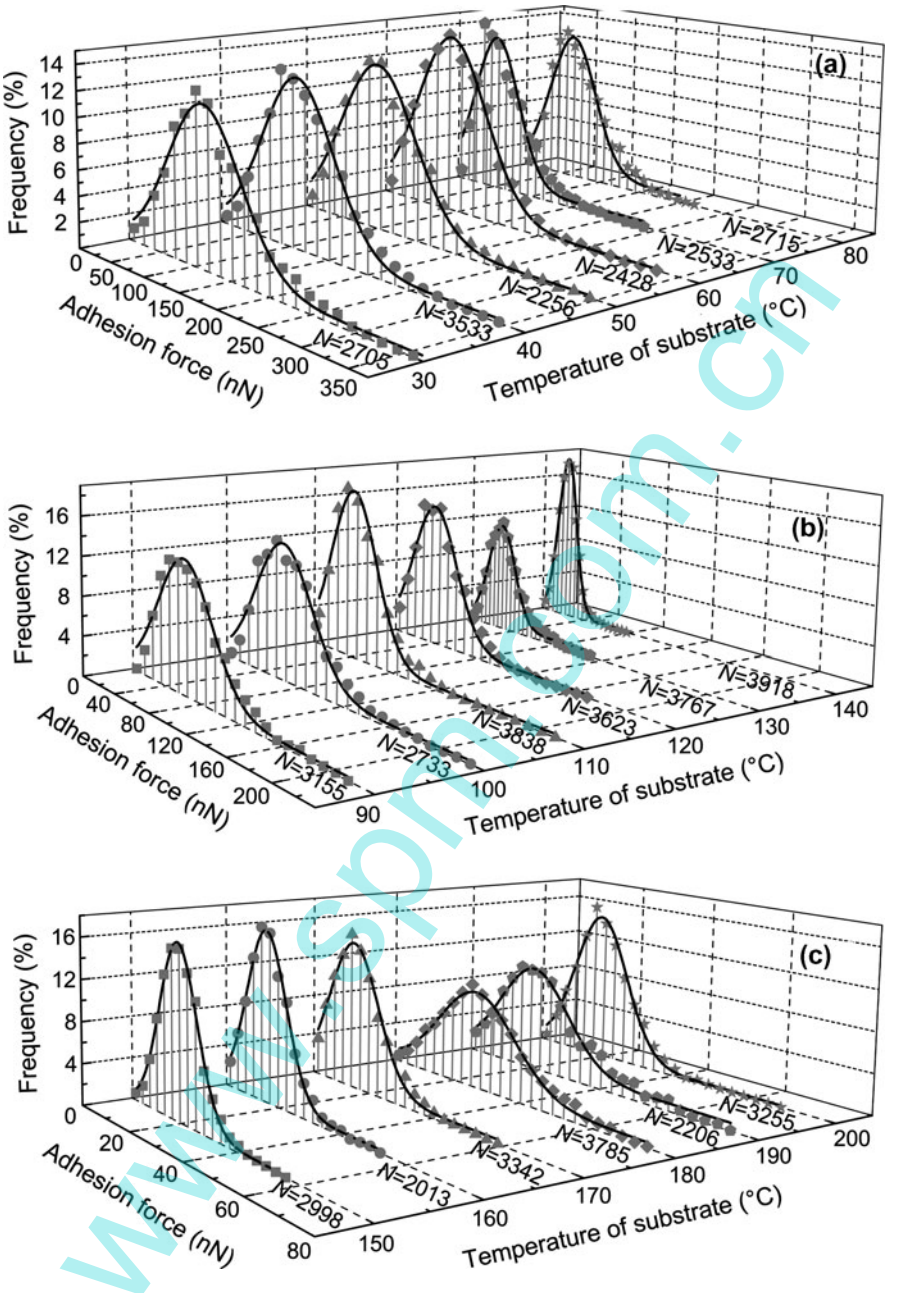

Figure 8. Histograms that show the distribution of adhesion force values for different temperatures in the glove box. (a) The temperatures are between 30 and 80 °C; (b) the temperatures are between 90 and 140 °C; and (c) the temperatures are between 150 and 200 °C. The numbers of the curves used are displayed beside the histograms.

30 °C. It is a typical force–displacement curve. The hysteresis of curve due to the adhesion force is obvious, although the feature of jumping into contact is not. The curve shown in Figure 6(b) was obtained at 130 °C. The voltage of the zero line is a little far

away from 0 V, although the voltage of photodetector was set to 0 V at the beginning of the experiment. The end of the cantilever bends downward when approaching the sample. The tip has not touched the sample when the Z voltage is the largest. Therefore, the adhesion force is not available from this curve. The curve shown in Figure 6(c) was obtained at 170 °C. It only shows the contact parts of the approach and retraction lines. The voltage of the zero line is not larger than −2 V. Therefore, the adhesion force is also not available. For another, the tip will move to the next point to collect a curve when the previous curve has been obtained. This will cause the extension or retraction of the scanner because of different topographies. This will also increase the possibility of obtaining some incorrect curves. Since the incorrect curves are not found when collecting curves at the same location, this influence factor is also important. We used a FORTRAN program to extract the values of the adhesion force from the force–displacement curves. The curves were first checked by the program. If a curve was not the typical one, it would be deleted and not be considered.

Figure 7 shows the adhesion force histograms for different temperatures under ambient conditions. Each of them exhibits a Gaussian-like distribution for different

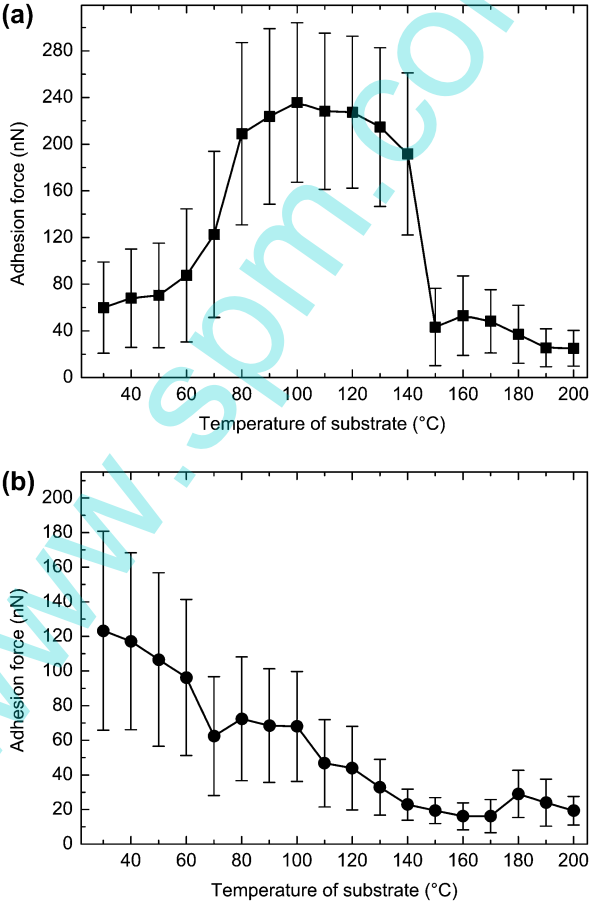

Figure 9. Adhesion force vs. the temperature of substrate using the flat tip (a) under ambient conditions and (b) in the glove box. Each point is an average of many measurements, the error bar being the standard deviation of each set of points.

temperatures (fitting curves displayed in the figure). Figure 8 shows adhesion force histograms for different temperatures in the glove box. The distributions are also Gaussian like. The numbers of the force–displacement curves used are displayed beside the histograms for different temperatures in Figures 7 and 8. A large number of curves were collected for a single temperature. This method is in accordance with the suggestion proposed by Noy that a successful experiment needs thousands of force–displacement curves.[21]

The mean adhesion forces and their standard deviations are shown in Figure 9 for different temperatures under both conditions. Under ambient conditions, the mean adhesion force first increases with the increase in temperature and reaches the maximum at ~100 °C. Then the mean adhesion force begins to decline slightly. At about 150 °C, the mean adhesion force decreases dramatically, and remains relatively stable at high temperatures. It can be seen that the temperature is increased from 30 to 100 °C and the mean adhesion force is increased by a factor of 4. However, in the glove box, the mean adhesion force decreases with increasing temperature. The mean adhesion force at 30 °C is about six times larger than that at 200 °C. It should also be noted that at high temperatures (180–200 °C), the mean adhesion forces under both conditions are almost the same.

Here, we first discuss the reason why the mean adhesion force increases below ~100 °C. Under ambient conditions, the capillary force is always present, and the van der Waals (vdW) force is relatively small when compared with the capillary force. Generally speaking, there are two water transport mechanisms in the formation of water capillary bridges between the tip and the sample: (1) condensation of water vapor in the gap and (2) adsorption of water molecules on the surface region around the contact and flow of thin water film toward the growing meniscus.[22–24]

Usually, the capillary condensation is viewed as two processes: capillary nucleation and subsequent growth of the meniscus to thermodynamic equilibrium by the diffusion of water molecules.[25] The nucleation is to create the nuclei which are larger than the critical size of water nanomeniscus by overcoming the activation energy barrier. If the nucleus is smaller than the critical size, the water nanomeniscus will be ruptured immediately because the meniscus is energetically unfavorable.[26] It means that the nucleation is at the initial stage of condensation.

The nucleation of the water nanomeniscus is a thermally activated process, and the nucleation rate Γ can be described by Arrhenius law [27]:

$$\Gamma = \Gamma_0 \exp\left(-\frac{\Delta\Omega^*}{k_B T}\right) \tag{2}$$

where Γ_0 is a prefactor, $\Delta\Omega^*$ is the activation energy barrier, T is the absolute temperature, and k_B is the Boltzmann constant ($1.3806505 \times 10^{-23}$ JK^{-1}). Here, we assume that $\Gamma_0 = 3.4 \times 10^8$ Hz, $\Delta\Omega^* = 7.65 \times 10^{-20}$ J. According to Equation (2), we get the relation of nucleation rate and the temperature, as shown in Figure 10. From this figure, the nucleation rate increases dramatically with the increase in temperature. Since the contact time between the tip and the sample is unchangeable, the increased nucleation rate will lead to more liquid bridges between asperities of the surfaces. Due to the increase in energy, liquid bridges can also be formed between asperities with longer distances. All of these will cause increased capillary force.

The elevated temperature can not only improve the nucleation rate, but also speed up the diffusion of water molecules. After the formation of the nanomeniscus, the

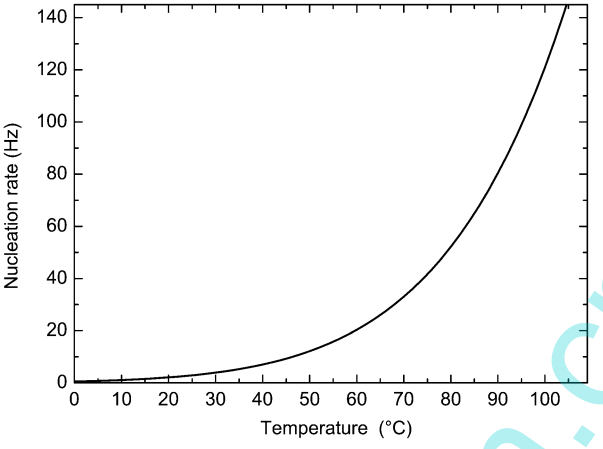

Figure 10. The relation of nucleation rate and temperature.

meniscus grows through condensation of the water vapor that diffuses in the gap. That means, the radius of the meniscus will continue to increase until the equilibrium is reached. There are three transport mechanisms: molecular diffusion, Knudsen diffusion, and surface diffusion. Each of them may play a part in the capillary condensation. Since the diffusions depend strongly on the structure character, we cannot make an accurate prediction of the total diffusivity. Usually, the mean-free path of the water molecules is approximately 100 nm, and the diffusion resistance is mainly from the collisions of water molecules against the tip and the sample. Therefore, the Knudsen diffusion is the main diffusion mode.[22,24] Dushman [28] proposed the Knudsen diffusion coefficient $C_K = 2D[2R_G T/(\pi M)]^{1/2}/3$, where D is the radius of the pore, R_G the universal gas constant, and M the molar mass of water. It can be seen that with the increase in temperature, the diffusion coefficient increases.

Obviously, the elevated temperature of the sample will raise the temperature of the atmosphere in the gap, and eventually result in increased diffusion. If the water vapor can be viewed as an ideal gas, the mean translational kinetic energy of the water vapor molecules is: $m_0\bar{v}^2/2 = 3k_B T/2$, where m_0 is the molecular mass and $\bar{v}$ is the average speed. Therefore, the elevated temperature will increase the velocity of the water molecules and they will reach the meniscus faster. Since the contact time between the tip and the sample is limited, the increased temperature will lead to larger and/or more numerous liquid bridges.

Under ambient conditions, the surfaces of the tip and the sample are all covered with adsorbed water layers. Since both surfaces are hydrophilic, the liquid bridge formed is concave. Young–Laplace equation can be used to describe pressure difference Δp across the surface. It is, $\Delta p = \gamma_L\left(r_1^{-1} + r_2^{-1}\right)$ where γ_L is the surface tension or surface energy of the liquid film, r_1 are r_2 the principal radii of curvature of the surface. It can be seen that the pressure inside the liquid is smaller than the gas pressure for a concave meniscus. If the film outside the contact zone is flat, the pressure difference between the outside and inside of interface is vanished. Therefore, the pressure inside the liquid of a concave meniscus is smaller than that of the surrounding water film. That means the surrounding water film will flow toward the growing meniscus and the elevated temperature will accelerate this kind of flow.

The probe is farther away from the heater than the sample, and the tip will snap out of contact with the sample once a single force–displacement curve is collected. Therefore, the temperature difference between the sample and the tip will lead to the temperature difference in the water film absorbed on them. The temperature gradient will cause the surface tension gradient. Since a liquid with a high surface tension pulls more strongly on the surrounding liquid than one with a low surface tension, the presence of a gradient in surface tension will naturally cause the liquid to flow away from regions of low surface tension (Marangoni effect). In the system of tip and sample, the liquid of the sample will flow toward the tip, and this also leads to larger and/or more numerous liquid bridges.

From the discussion above, the capillary nucleation, the diffusion of water molecules, and the flow of thin water film toward the growing meniscus are all related to the temperature. The elevated temperature will lead to larger and/or more numerous liquid bridges, and eventually lead to larger adhesion force.

Meanwhile, it should also be noted that the capillary force is directly related to the surface tension. The elevated temperature will reduce the surface tension of water. When the temperature rises from 30 to 100 °C, the surface tension reduces by 21.4%.[29] It seems that the factor of reducing surface tension is unimportant when comparing with the factor of the numbers and the radius of the liquid bridges.

When the temperature of the sample is larger than ~100 °C, the water film will begin to evaporate. However, the formation of the liquid bridges does not stop completely. It can be seen from Figure 9, between 100 and 140 °C, the adhesion force reduced slightly. When the temperature reaches ~150 °C, the mean adhesion force reduces sharply and remains relatively small at high temperatures. At high temperatures, the capillary force may no longer be the major contribution to the adhesion force, and becomes less important. This may attribute to the decrease in the radius of the liquid bridges or no liquid bridges at all. The adhesion force is mainly contributed by the vdW interaction. That is why the mean adhesion forces under ambient conditions and in the glove box are almost the same at high temperatures.

In the glove box, the capillary force will disappear, and the vdW force becomes the dominant force. And the electrostatic forces may become the second important contributor. The elevated temperature increases the vibrational energy of atoms on the surface, and eventually vdW bonds are broken. We can also see that from the three components of the vdW potential. The potentials are the orientation potential, the induction potential, and the dispersion potential. The orientation potential between atoms and/or molecules can be expressed as $w_K(l) = -u_1^2 u_2^2 / \left[3(4\pi\varepsilon_0\varepsilon)^2 k_B T d^6\right]$, where u_1 and u_2 are the dipole moments of the molecules, ε_0 is the dielectric constant in vacuum, ε is the dielectric constant of the medium, and d is the distance. The elevated temperature will lower the orientation potential. The induction potential is irrelevant with temperature. The elevated temperature will lead to larger distance between molecules, and eventually lead to weaker intermolecular forces. Therefore, it will lower the dispersion potential to some extent. It should be noted that our experiment results in the glove box are consistent with the results proposed by Shavezipur et al. [13].

4. Conclusions

In this work, the influence of temperature on the microscale adhesion force has been studied with an AFM under ambient conditions and in dry nitrogen. The substrate temperature was varied between 30 and 200 °C. The outcomes show that when the

temperature is less than 200 °C, the influence of temperature on the normal spring constant of the cantilever can be ignored. In this temperature range, the adhesion forces' distribution for each temperature exhibits a Gaussian-like distribution under both situations. Under ambient conditions, the mean adhesion force first increases with the increase in temperature and reaches the maximum at ~100 °C. The increase in adhesion is associated with the capillary force. The elevated temperature will lead to larger and/or more numerous liquid bridges. The capillary nucleation, the diffusion of water molecules, and the flow of thin water film are all enhanced with the elevated temperature. Between 100 and 140 °C, the adhesion force reduced slightly. That means the water film begins to evaporate, but the formation of the liquid bridges continues. At about 150 °C, the adhesion force decreases dramatically and remains relatively stable at high temperatures. At high temperature, the vdW force becomes the dominant contribution to the adhesion force. However, in dry nitrogen, the mean adhesion force decreases with the increase in temperature. This trend is attributed to the broken van der Waals bonds. Due to the same major contribution to the adhesion force, the mean adhesion forces at high temperatures are almost the same.

Funding

The work was supported by the National Natural Science Foundation of China [grant number 51175182].

References

[1] Kim SH, Asay DB, Dugger MT. Nanotribology and MEMS. Nano Today. 2007;2:22–29.
[2] Grierson DS, Konicek AR, Wabiszewski GE, Sumant AV, de Boer MP, Corwin AD, Carpick RW. Characterization of microscale wear in a polysilicon-based MEMS device using AFM and PEEM–NEXAFS spectromicroscopy. Tribol. Lett. 2009;36:233–238.
[3] Fischer HR, Gelinck ERM. Determination of adhesion forces between smooth and structured solids. Appl. Surf. Sci. 2012;258:9011–9017.
[4] Ando Y. The effect of relative humidity on friction and pull-off forces measured on submicron-size asperity arrays. Wear. 2000;238:12–19.
[5] Ando Y. Effect of contact geometry on the pull-off force evaluated under high-vacuum and humid atmospheric conditions. Langmuir. 2008;24:1418–1424.
[6] Ferreira ODS, Gelinck E, de Graaf D, Fischer H. Adhesion experiments using an AFM-parameters of influence. Appl. Surf. Sci. 2010;257:48–55.
[7] Çolak A, Wormeester H, Zandvliet HJW, Poelsema B. Surface adhesion and its dependence on surface roughness and humidity measured with a flat tip. Appl. Surf. Sci. 2012;258:6938–6942.
[8] Çolak A, Wormeester H, Zandvliet HJW, Poelsema B. The influence of instrumental parameters on the adhesion force in a flat-on-flat contact geometry. Appl. Surf. Sci. 2014;308:106–112.
[9] Lai T, Huang P. Study on microscale adhesion between solid surfaces with scanning probe. Sci. China Technol. Sci. 2013;56:2934–2952.
[10] Nelson BA, Poggi MA, Bottomley LA, King WP. Temperature-dependence of water bridge formation in atomic force microscopy. In: Proceedings ASME 2003 International Mechanical Engineering Congress and Exposition, American Society of Mechanical Engineers; 2003 November 15–21; Washington, DC. p. 629–636.
[11] Tambe NS, Bhushan B. Scale dependence of micro/nano-friction and adhesion of MEMS/NEMS materials, coatings and lubricants. Nanotechnology. 2004;15:1561–1570.
[12] Awada H, Noel O, Hamieh T, Kazzi Y, Brogly M. Contributions of chemical and mechanical surface properties and temperature effect on the adhesion at the nanoscale. Thin Solid Films. 2011;519:3690–3694.

[13] Shavezipur M, Gou W, Carraro C, Maboudian R. Characterization of Adhesion Force in MEMS at High Temperature Using Thermally Actuated Microstructures. J. Microelectromech. Syst. 2012;21:541–548.
[14] Cappella B, Stark W. Adhesion of amorphous polymers as a function of temperature probed with AFM force–distance curves. J. Colloid Interface Sci. 2006;296:507–514.
[15] Xie J, Xie HF, Liu XR, Tan TW. Dry micro-grooving on Si wafer using a coarse diamond grinding. Int. J. Mach. Tools Manuf. 2012;61:1–8.
[16] Butt HJ, Cappella B, Kappl M. Force measurements with the atomic force microscope: technique, interpretation and applications. Surf. Sci. Rep. 2005;59:1–152.
[17] Carpick RW, Batteas J, Boer MPd. Scanning probe studies of nanoscale adhesion between solids in the presence of liquids and monolayer films. In: Bhushan B, editor. Springer handbook of nanotechnology. Heidelberg: Springer; 2007. p. 951–980.
[18] Watanabe H, Yamada N, Okaji M. Linear thermal expansion coefficient of silicon from 293 to 1000 K. Int. J. Thermophys. 2004;25:221–236.
[19] Chun Hyung C. Characterization of Young's modulus of silicon versus temperature using a "beam deflection" method with a four-point bending fixture. Curr. Appl. Phys. 2009;9:538–545.
[20] Rao SS. Mechanical vibrations. 4th ed. New York (NY): Pearson Education; 2004.
[21] Noy A. Force spectroscopy 101: how to design, perform, and analyze an AFM-based single molecule force spectroscopy experiment. Curr. Opin. Chem. Biol. 2011;15:710–718.
[22] Wei Z, Zhao Y-P. Growth of liquid bridge in AFM. J. Phys. D: Appl. Phys. 2007;40:4368–4375.
[23] Rabinovich YI, Singh A, Hahn M, Brown S, Moudgil B. Kinetics of liquid annulus formation and capillary forces. Langmuir. 2011;27:13514–13523.
[24] Sirghi L. Transport mechanisms in capillary condensation of water at a single-asperity nanoscopic contact. Langmuir. 2012;28:2558–2566.
[25] Sung B, Kim J, Stambaugh C, Chang SJ, Jhe W. Direct measurement of activation time and nucleation rate in capillary-condensed water nanomeniscus. Appl. Surf. Sci. 2013;103:213107.
[26] Restagno F, Bocquet L, Biben T. Metastability and nucleation in capillary condensation. Phys. Rev. Lett. 2000;84:2433–2436.
[27] Szoszkiewicz R, Riedo E. Nucleation time of nanoscale water bridges. Phys. Rev. Lett. 2005;95:135502.
[28] Dushman S. Scientific foundations of vacuum technique. New York (NY): Wiley; 1949.
[29] Vargaftik NB, Volkov BN, Voljak LD. International tables of the surface tension of water. J. Phys. Chem. Ref. Data. 1983;12:817–820.